NATIONAL ADVISORY COMMITTEE FOR AERONAUTICS

TECHNICAL NOTE 3219

VISCOSITY CORRECTIONS TO CONE PROBES IN RAREFIED SUPERSONIC FLOW AT A NOMINAL MACH NUMBER OF 4

By L. Talbot

University of California

Washington
November 1954

NATIONAL ADVISORY COMMITTEE FOR AERONAUTICS

TECHNICAL NOTE 3219

VISCOSITY CORRECTIONS TO CONE PROBES IN RAREFIED SUPERSONIC FLOW AT A NOMINAL MACH NUMBER OF 4

By L. Talbot

SUMMARY

Data were obtained for the viscosity corrections to cone probes in supersonic rarefied air flow at a nominal Mach number of 4. The test models consisted of a set of seven geometrically similar 5° semivertex-angle cones. Additional experiments were made to determine cone surface pressure distributions and the effects resulting from the variable orifice size on the geometrically similar models. The results indicate that the viscous effects are quite complex and depend not only on the distance from the cone vertex to the pressure orifice but also on the size of the pressure orifice and the location of the orifice with respect to the shoulder. Pressure distributions near the vertex were compared with the tangent-cone and linearized theories. The experimental pressure coefficients were higher than the linearized theory but considerably lower than the more exact tangent-cone theory.

Tables are presented for 5° semivertex-angle cones giving free-stream Mach numbers and static pressures in terms of the ratio of impact and cone surface pressures over the range $1.10 \leq M_1 \leq 5.99$.

INTRODUCTION

The determination of the flow conditions in a supersonic wind tunnel requires two local measurements if the expansion from the stagnation chamber to the test section is not isentropic. One procedure is to measure the impact pressure p_{1t}' and a cone pressure p_2 at the same point in the flow. Since the ratio p_{1t}'/p_1 is given as a function of M_1 through the normal-shock-wave theory, while the ratio p_2/p_1 is given in terms of M_1 by the Taylor-Maccoll conical-flow relationships, two simultaneous equations are obtained for the unknowns p_1 and M_1 in terms of the measured quantities p_{1t}' and p_2 which are readily solved by use of existing tables. Details of the method and calculated results for $1.10 \leq M_1 \leq 5.99$ are presented in appendix A and table I.

At the low Reynolds numbers which obtain in rarefied gas flows the measured impact and cone pressures depart from their ideal flow values. The viscous corrections which must be applied to measured impact pressures have been the subject of several recent theoretical and experimental investigations (refs. 1 through 7). These investigations have, among other things, yielded empirical viscosity-correction curves for impact probes of several shapes and have shown that viscosity effects are negligible for diameter Reynolds numbers greater than about 200. There are available at present, however, few or no data of a similar nature for cone probes.

The purpose of this report is to present viscosity-correction data at a nominal Mach number of 4 for one particular family of geometrically similar cone probes. The investigations also included the determination of cone surface pressure distributions and measurements to obtain an estimate of the effect of variation in pressure-orifice diameter on the measurement of cone surface pressure.

This work was conducted at the University of California under the sponsorship and with the financial assistance of the National Advisory Committee for Aeronautics and was under the immediate supervision of Professors R. G. Folsom and S. A. Schaaf of the Department of Engineering at Berkeley.

SYMBOLS

a,b	functions of θ (see eq. (B5))
C_p	pressure coefficient, $\frac{p_2 - p_1}{\rho_1 u_1^2/2}$
C_p'	pressure coefficient, $(p_2/p_{2i}) - 1$
D	base diameter of cone
d	diameter of pressure orifices on cone
$f(M_1,\theta)$	function defined by equation (B19)
K	similarity parameter, $\frac{M_1}{l/D}$
l	axial length of cone

M	Mach number
n	power of Reynolds number
p	pressure
p_{1t}	total or stagnation pressure corresponding to free-stream conditions
p_{1t}'	stagnation pressure behind a normal shock wave (as measured by an impact tube in free stream)
Δp_2	difference between measured cone surface pressure and that value obtained by extrapolating to zero pressure-orifice diameter
R	gas constant
$(Re_x)_1$	Reynolds number, $u_1 x/\nu_1$
$(Re_x)_2$	Reynolds number, $u_2 x/\nu_2$
r	radius of "effective body" (cone plus displacement thickness)
r_o	radius of cone
S	cross-sectional area of effective body
T	temperature, $^\circ R$ abs
u	stream velocity
x	distance measured along cone surface from vertex
γ	specific-heat ratio, 1.400
δ^*	boundary-layer displacement thickness
θ	cone semivertex angle
μ	coefficient of viscosity
ν	kinematic viscosity of fluid
ξ	distance measured along cone center line from vertex
ρ	density of fluid

Subscripts:

1	free-stream conditions
2	conditions on cone surface or at boundary-layer seam behind conical shock wave
e	value obtained by extrapolation to zero pressure-orifice diameter
i	ideal conditions, obtained for infinite Reynolds number
s	pertaining to conditions at cone shoulder
t	total or stagnation conditions
x	pertaining to distance measured along cone surface from vertex

APPARATUS AND PROCEDURE

Wind Tunnel

The tests were conducted in an open-jet continuous-flow type of wind tunnel (no. 3 wind tunnel, ref. 8) using supersonic nozzle 8, with a nominal Mach number of 4. The nozzle is of the axisymmetric type and was designed by methods described in references 9 and 10. The wind tunnel is equipped with an eight-faced rotary probe selector (ref. 7) which allowed the consecutive testing of seven cone models and an impact probe (used for determination of the Mach number) without opening the tunnel to the atmosphere.

Models

All cones were of 5° semivertex angle. Three different types were tested. The type A cones were preliminary models designed to obtain surface pressure distributions and consisted of a set of 14 probes of equal size. Each cone had four pressure orifices of 0.015-inch diameter spaced at 90° intervals around its circumference, located at varying distances from the vertex as shown in figure 1.

The basic test models consisted of a set of seven geometrically similar cones, designated as type B. Each cone had four pressure orifices spaced at 90° around its circumference and located at an axial distance midway between the vertex and the shoulder. The pressure-orifice diameters

were scaled up in the same geometric ratio as the other cone dimensions; orifice diameters ranged from 0.020 inch on the smallest model to 0.100 inch on the largest. These models are shown in figures 2 and 3.

A third set of seven cones, designated as type C, was tested in an attempt to determine independently the effects which resulted from the variation in orifice diameter on the type B models. The type C cones had common dimensions and axial locations of the pressure orifices, but had pressure-orifice diameters ranging from 0.020 inch to 0.150 inch. Specifications for the type C cones are given in figure 4.

All models were leak-tested and outgassed before being run. Time responses of the various probe-system configurations were measured to obtain the time intervals necessary for pressure equilibrium.

Pressure Measurement Instrumentation

The reference instrument for all pressure measurements was a mercury McLeod gage (ref. 7) with a least count of 0.001 inch of mercury. The probable error in McLeod readings converted to absolute pressure is less than 1 percent. However, only one flow quantity, the Reynolds number, is dependent on the absolute pressure. Flow quantities which involve Mach number are determined by measurements of pressure ratios, and the appropriate index of accuracy of the McLeod gage for this type of measurement is the probable error in the measurement of two nearly equal pressures. This error was calculated to be from 0.12 percent to 0.03 percent over the pressure range 35 to 850 microns of mercury, the larger pressure being the upper limit of the instrument.

Besides its use for calibration purposes the McLeod gage was employed for direct measurements of test chamber and nozzle wall pressures and in some cases for measurements of cone surface pressures. The use of the McLeod gage for all pressure measurements was precluded by range and time-constant limitations.

A precision butyl phthalate oil manometer (ref. 11) was used for measurements of impact and stagnation chamber pressures. This manometer had a least count of 0.001 inch of oil, equivalent to approximately 2 microns of mercury, and gave readings which were reproducible to about one-half the least count. The manometer was calibrated against the McLeod gage to avoid the difficulties introduced by the different temperature - specific-gravity corrections for mercury and the manometer oil.

Cone surface pressures were measured in most cases by means of a temperature-controlled thermistor manometer (Western Electric thermistor manometer D-176255) in a suitable bridge circuit with bridge unbalance

measured by a 0- to a 10-millivolt Brown precision potentiometer. Zero suppression was accomplished with a 0- to 10-volt potentiometer in series with the Brown instrument. For the pressure range encountered in the present tests the 0.02-millivolt least count of the Brown potentiometer corresponded to a pressure increment of about 0.004 micron. Analysis of the calibration data yielded a maximum probable error of about 1 percent for pressures measured with the thermistor. As a check on this estimate the type C cones were tested at one flow rate using both the thermistor and the McLeod gage for pressure measurements. Discrepancies in level between the pairs of measurements were less than 1 percent.

Tunnel Calibration

Free-stream Mach numbers and static pressures were determined by measurements of impact and stagnation-chamber pressures; M_1 is found from p_{1t}'/p_{1t} by use of normal-shock-wave tables (ref. 12). Inherent in this method is the assumption of isentropic flow between the stagnation chamber and the test region, that is, that $p_{stag} = p_{1t}$. The validity of this assumption has been borne out by extensive nozzle evaluation tests which are reported in reference 10. These tests showed that the jet core was adiabatic and shock-free, with a maximum variation of $\pm\frac{1}{2}$ percent in the impact pressure within the test cone. Measured wall tap pressures at the exit agreed within experimental error with static pressures calculated from measured values of p_{1t}'/p_{1t} and the isentropic-flow assumption. Moreover, the design Mach number was almost perfectly attained at the design flow rate $\left(M_{theor} = 4.00 \text{ and } M_{exp} = 3.98\right)$.

All data presented in this report were obtained with the cone models located on the nozzle axis so that the surface pressure orifices coincided with the exit plane of the nozzle, necessitating different locations of the cone vertices. Tranverses made with a cone and an impact tube showed that where axial Mach number gradients were present the most consistent results were obtained when the nose of the impact tube and the cone pressure orifices were at the same axial location. Some additional tests made with models at off-axis and different axial positions are discussed in the section "Calibration Data for Geometrically Similar Cones (Type B)."

Impact-pressure measurements were made with a 0.300-inch-diameter source-shaped impact probe, with viscosity corrections applied as in reference 7.

RESULTS

Cone Surface Pressure Distributions (Type A Models)

The data for the preliminary tests on the type A cones are presented in table II. The results are presented graphically in figures 5 and 6. The pressure coefficient is defined by $C_p' = \frac{p_2 - p_{2i}}{p_{2i}}$, with ideal cone pressures obtained from table I. In figure 6 C_p' has been divided by the function $f(M_1,\theta)$ defined by equation (B19) to facilitate later comparisons with the theory presented in appendix B. The Reynolds number is based on free-stream velocity and kinematic viscosity and the distance along the cone surface from the vertex.

Calibration Data for Geometrically Similar Cones (Type B Models)

Results for the geometrically similar cones (type B models) are presented in table III and are plotted in figure 7. The pressure coefficient C_p' is defined as before, and the Reynolds number is based on free-stream velocity and viscosity. Pressure coefficients obtained for the smallest model (B1) are included in table III, but have not been plotted in figure 7. The reason for this is discussed in the section "Calibration Data for Geometrically Similar Cones (Type B)."

Orifice Size Effect (Type C Cones)

The orifice-size-effect data for the type C cones are tabulated in table IV and are plotted in figure 8. Results are presented for nominal Mach numbers of 2 and 4 (see the section "Tests at Other Mach Numbers"). In figure 8 the quantity Δp_2 represents the difference between the measured cone pressure and the value obtained by extrapolation to zero orifice diameter.

Tests at Other Mach Numbers

The test program was repeated using nozzle 6, which is an axisymmetric nozzle with nominal Mach number of 2 ($1.95 < M_1 < 2.20$; $158 < u_1/\nu_1 < 763$/inch). The data obtained in this nozzle for the type A and type B models exhibited the same trends as the previous data obtained in nozzle 8. The results at Mach number 2 were regarded as only qualitative, however, because of the large uncertainty in Mach number

determination (about 4 percent). For this reason only the type C model data, which are relatively insensitive to errors in Mach number determination, are presented.

DISCUSSION

Type A Models

Before proceeding to the discussion of the calibration data for the geometrically similar models, it will be helpful to examine some of the results obtained for cone surface pressure distributions with the type A models.

The distributions of surface pressures shown in figure 5 are in qualitative agreement with what might be expected for a cone with a thick boundary layer, the surface pressure being highest near the vertex and trending toward the ideal pressure with increasing x. A decided "shoulder effect" is apparent in all these pressure distributions, evidenced by a decrease in pressure on the cone near the juncture between the cone surface and the cylindrical afterbody.[1] The extent of upstream influence of the shoulder expansion appears to be of the order of three to five times δ_s^*, the calculated undisturbed boundary-layer displacement thickness at the shoulder. This result might be compared with the experiments on shock-wave interaction with laminar boundary layers on flat plates. Ackeret, Feldman, and Rott (ref. 13) found that the disturbance caused by a 3° compression wave incident on a flat-plate laminar boundary layer at $M_1 = 2$ extended upstream some 50 displacement thicknesses. Similar orders of magnitude were found by Lee (ref. 14) on cylindrical bodies.

---

[1]The break in the distributions between cones A7 and A8 is not shoulder effect, but can be traced to the probable errors in thermistor calibration and flow determination, since models A1 to A7 and A8 to A14 were tested separately. The greater amount of scatter in the data for models A8 to A14 is due to the fact that these pressures were measured with the oil manometer, whereas the pressures on models A1 to A7 were measured with the thermistor manometer. The oil manometer has a least count of about 1 micron of mercury, as compared with the 0.004-micron least count of the thermistor manometer. However, calibration repeatability with the oil manometer was slightly better than that with the thermistor manometer. The absolute pressure level indicated by the oil-manometer data is probably slightly more reliable, and therefore the indicated values of $C_p' = \left(p_2/p_{2i}\right) - 1$ obtained for models A1 to A7 at the lower flow rates are possibly a little low.

Calibration Data for Geometrically Similar Cones (Type B)

The data for the geometrically similar cones (fig. 7) exhibit the anticipated general trend with Reynolds number. These pressure coefficients are somewhat higher than those obtained with the type A cones at the same Reynolds numbers because of the hole-size effect discussed in the section "Orifice Size Effect." An estimate of the maximum probable error in $C_p' = p_2/p_{2i} - 1$ can be obtained by applying the 1-percent maximum probable error in p_2 to the data of table III. For the data presented in figure 7, the maximum probable error in C_p' is approximately ±5 percent. The corresponding maximum probable error in p_{2i} is ±1 percent.

The results obtained with the smallest cone (B1) have not been included in figure 7. This probe gave pressure readings which were consistently high and did not correlate with other data at the same value of $(Re_x)_1$. These higher pressures may be due in part to thermal creep effects. The mechanism of thermal creep is discussed in reference 15, where it is shown that a temperature in a tube containing gas at rest will set up a pressure gradient given by

$$\Delta p = \frac{24\overline{\mu^2}R}{D^2\bar{p}} \Delta T \qquad (1)$$

where Δp and ΔT represent the difference in pressure and temperature, respectively, between the ends of the tube; R, the gas constant; $\overline{\mu^2}$, the average square of the viscosity over the temperature range; D, the internal diameter of the tube; and $\bar{p}$, the mean pressure in the tube.

The existence of temperature gradients in the tubular afterbody of the test models is explained by the fact that the cone surface recovery factor[2] is about 0.83 (ref. 16), whereas a major portion of the model support, which connects to the downstream end of the tube, is outside the jet and at stagnation temperature. Because of conduction through the model support the downstream end of the tube is at a temperature somewhere between the recovery temperature and the stagnation temperature. The actual temperature differences measured with thermocouples installed on model B1 were approximately 25° F at a flow rate of 5.2 pounds per hour and 40° F at a flow rate of 20 pounds per hour. Using these temperature differences, Δp was calculated for model B1 (internal diameter, 0.085 inch) and found to be about 2 microns of mercury at both flow rates.

---

[2]This is the corrected recovery factor. The actual cone equilibrium temperature will be somewhat higher because of radiation and conduction heating.

Although the trend is in the right direction, the calculated pressure differences due to thermal creep are not large enough to explain completely the high pressures obtained with probe B1.

An interesting feature exhibited in the type B probe data is the pressure "bump" which occurred on either probe B4 or probe B5. This reversal in the variation of C_p' with $(Re_x)_1$ was also observed at every flow rate in nozzle 6. At first it was believed that this pressure reversal might be due to either a leak or an imperfection in one of the probes. The probes were retested for leaks and examined under a glass and were found to be satisfactory. Moreover, it was observed that at the highest flow rates the bump shifted from probe B4 to B5, which indicated that the effect was not unique to one probe. The probes were also tested at off-axis and different axial positions to determine whether the observed pressure reversal was caused by tunnel gradients. In every case the same characteristic reversal was found.[3] It is believed that the pressure reversal observed on models B4 and B5 may be due to the upstream transmission of the shoulder expansion through the laminar boundary layer. That is, the pressure orifices on the smaller models B2 and B3 might all have been within a zone of reduced surface pressures near the shoulder. The distance from the shoulder to the pressure orifices on model B5 was 0.906 inch, which is of the order of the maximum extent of upstream influence noticed on the type A probes.

Some additional tests were made to determine how much the disturbance produced by the model support affected the measured cone pressures. A model with the same cone dimensions as B1 but with an afterbody one and one-half times as long was tested together with B1. The difference in pressures on these two models was within the probable error of measurement, and it was concluded that support interference was negligible.

Orifice Size Effect

The data plotted in figure 8 and tabulated in table IV show an increase in measured pressure with orifice diameter. The equation

$$\Delta p_2 = 15.5 \sqrt{M_1}\, d \qquad (2)$$

---

[3]The off-axis tests also established the fact that the flow was sufficiently uniform near the axis, so that no appreciable error was introduced on the larger probes for which the pressures sensed at the orifices corresponded to points in the flow which were some distance off-axis when the probes were on center line.

where Δp_2 is in microns of mercury and d is in inches, represents a crude attempt to correlate the data and is presented only as a suggestion of the possible dependence of Δp_2 on M_1. Some of the scatter in the data is probably due to imperfections in the pressure orifices. The hole-size correction is appreciable; the pressure coefficient C_p' for probe B7 at the lowest flow rate would be decreased by 32 percent if equation (2) were used to correct the measured p_2.

It was interesting to note that for approximately constant Mach number Δp_2 was insensitive to changes in static-pressure level and hence to changes in mean free path in the gas. From this it may be inferred that the orifice size effect might be a "ram" effect and not a viscous effect nor a rarefaction phenomenon associated with large mean free path.

These results on orifice size serve only as a qualitative indication of the type of correction which will have to be considered in any theory developed to predict pressure coefficients for families of geometrically similar "static probes." A much more detailed experimental program, including the effect of varying d/x ratio, will be necessary before the hole-size correction is known to any degree of precision.

Comparison With Theory for an Infinite Cone

The linearized theory of appendix B gives the result $C_p' = \frac{f(M_1,\theta)}{\sqrt{(Re_x)_2}}$, where $f(M_1,\theta)$ is a function of the free-stream Mach number and the semivertex angle of the cone and $(Re_x)_2$ is the Reynolds number based on conditions which obtain at the boundary-layer seam. Figure 6 shows a comparison between this theory and the type A cone data. The agreement is fair except in the vicinity of the shoulder. In figure 6 the quantity $C_p'/f(M_1,\theta)$ has been plotted against $1/\sqrt{(Re_x)_1}$ rather than $1/\sqrt{(Re_x)_2}$. Only a slight difference is involved in this procedure, of the order of 1 percent or less, and data reduced on this basis are much easier to use.

Figure 9 shows a comparison between the "tangent-cone"[4] method and the linearized theory for one particular flow. The experimental pressure coefficients lie between the results of the two theories, being some 20 percent higher than the linearized theory but lower by a factor of 2 than the more exact tangent-cone theory. Ehret (ref. 18) has made comparisons between various approximation methods and the method of characteristics and has shown that the tangent-cone method gives only slightly higher pressure coefficients than the characteristics method on a tangent ogive for $M_1 = 3$ and the similarity parameter $K = \frac{M_1}{l/d} = 1$. (For the case shown in fig. 9, $K = 0.65$ if the cone geometry is uncorrected for boundary-layer effect, but has the value $K = 1.1$ if the calculated displacement thickness at the shoulder is added to the cone dimensions.) Ehret further shows that pressure coefficients derived from linearized theory are appreciably lower than the exact theory near the vertex of the cone and are higher than the exact theory far back on the body.

The fact that the linearized theory is in better agreement with experiment than the tangent-cone approximation is probably only a fortuitous circumstance, since the boundary-layer theory used to calculate δ^* cannot be applied with confidence below about $(Re_x)_2 = 10^5$. The large disparity between the linearized theory and the tangent-cone approximation (which should yield better results were the calculated δ^* reasonably close to correct) could mean that the method of correcting the external flow field for viscosity by the addition of a boundary-layer displacement thickness may be qualitatively correct, but not sufficiently precise for quantitative use. An alternative explanation, one for which there is considerable experimental evidence, is that the boundary layer near the vertex is considerably thinner than that predicted by conventional boundary-layer theory. Any conclusion with respect to such questions, however, must be deferred until additional experimental results are obtained and much more careful boundary-layer calculations including the effects of slip and pressure gradient are used to replace the simplified analysis of appendix B.

---

[4]The tangent-cone method consists in using the pressure coefficients for cones of semivertex angle equal to the angle of the composite body (cone plus boundary layer) at various stations. For pointed bodies of revolution this method can be employed either with local values of p_{2t}/p_{1t} or with the value of p_{2t}/p_{1t} which obtains immediately behind the conical shock. In the case at hand, the boundary-layer slope at $x = 0$ is infinite; therefore, the method using local values of p_{2t}/p_{1t} was employed. For the same reason the second-order theory of Van Dyke (ref. 17) could not be employed.

Extrapolation Method for Determination of Ideal Cone Pressure

In previous reports dealing with viscous corrections to impact pressures (refs. 1, 2, and 7) a technique was employed wherein the ideal impact pressure was determined by extrapolating the data to infinite Reynolds number. At the start of the present investigation it was hoped that a similar method could be used to determine p_{2i}, especially for nozzle 6 (nominal Mach number of 2) in which the isentropic-flow assumption has not been well substantiated. However, the errors involved in this method proved to be too great, and it was not employed. It can be seen in figures 5 and 7 that determination of p_{2i} by extrapolation (i.e., $x \to \infty$) would be most uncertain, although the data do appear to approach a value of C_p' only slightly greater than zero.

CONCLUDING REMARKS

The results obtained with geometrically similar cones are presented as calibration data for this type of cone probe in low-density supersonic flow. The corrections are quite complex in nature. The extent of upstream influence of the shoulder expansion becomes important for small cone probes, while the hole-size effect becomes appreciable for large probes. Each of these effects requires further investigation.

Experimental pressure distributions near the vertex of an infinite cone are in qualitative agreement with theoretical results obtained from analysis of ideal flow around the composite body formed by the cone plus boundary-layer displacement thickness. Experimental pressure coefficients were about 20 percent higher than the linearized theory, but lower by a factor of 2 than the more exact tangent-cone theory.

University of California,
Berkeley, Calif., June 1, 1953.

APPENDIX A

DETERMINATION OF FREE-STREAM CONDITIONS THROUGH IMPACT AND CONE PRESSURE MEASUREMENTS

Determination of the flow conditions in a supersonic stream requires two local measurements if the flow is not isentropic. One method is to measure the impact pressure p_{1t}' and a cone surface pressure p_2 at the same point in the flow. Thus, if M_1 and p_1, the undisturbed free-stream Mach number and static pressure, are considered as unknowns, two equations are obtained relating these unknowns to the known quantities p_{1ti}' and p_{2i} (the subscript i indicating that the measured impact and cone pressures have been corrected for viscosity effects).

The Rankine-Hugoniot normal-shock-wave theory (ref. 12) gives the result

$$\frac{p_{1ti}'}{p_1} = \left[\frac{2}{(\gamma + 1)M_1^2}\right]^{\frac{\gamma-1}{\gamma}} \left[\frac{2\gamma M_1^2 - (\gamma - 1)}{\gamma + 1}\right]^{\gamma-1} \tag{A1}$$

The function on the right-hand side of equation (A1) is tabulated up to $M_1 = 5.00$ in reference 12; values for higher values of M_1 are easily obtained by direct computation.

A relationship between the ideal cone pressure p_{2i} and the unknowns M_1 and p_1 is provided by the Taylor-Maccoll theory (ref. 19) which gives p_{2i}/p_1 as a function of M_1 and θ, the cone semivertex angle. The Taylor-Maccoll relationships cannot be written in closed form, however, and numerical integrations are necessary to obtain solutions. These integrations have been performed by Kopal (ref. 20) for different values of M_1 and for various values of θ. For the present application θ was taken equal to 5° and from the Kopal tables a chart was constructed giving p_{2i}/p_1 as a continuous function of M_1. These values were combined with equation (A1) to yield a unique relationship between M_1 and p_{1ti}/p_{2i} for a 5° semivertex-angle cone in supersonic flow with attached shock wave. Results for $1.10 \leq M_1 \leq 5.99$ are presented in table I.

APPENDIX B

BOUNDARY-LAYER EFFECT ON SURFACE PRESSURE OF AN INFINITE CONE IN SUPERSONIC FLOW[5]

ANALYSIS

The cone considered is oriented parallel to the direction of flow in the undisturbed free stream, its axis of symmetry in the ξ-direction and its vertex at the origin, as shown in figure 10. The semivertex angle is θ.

The linearized supersonic flow is considered to take place around a body consisting of the cone plus the displacement thickness of the boundary layer. The radius of this body is

$$r = \xi \tan \theta + \delta^* \sec \theta \tag{B1}$$

In reference 22 it is shown that the integration of the laminar-boundary-layer equation for a cone can be based on the results obtained for a flat plate and that, in particular,

$$\delta^* = (\delta^*)_{cone} = \frac{(\delta^*)_{plate}}{\sqrt{3}} \tag{B2}$$

where δ^* is calculated from the "local" properties of the potential flow at the cone surface. This calculation, under the assumptions that μ is proportional to T, that the Prandtl number is unity, and that the specific-heat ratio of the gas is 1.400, may be obtained from reference 23. The result is

$$(\delta^*)_{plate} = 1.73(1 + 0.277M_2^2)\left(\frac{\nu_2 x}{u_2}\right)^{1/2} \tag{B3}$$

---

[5]The analysis which follows is taken from a report by Lin, Schaaf, and Sherman (ref. 21). This report did not receive wide circulation; hence for convenience the major portion is reproduced here.

where the subscript 2 refers to the aforementioned local conditions on the cone surface. For the cone $x = \xi \sec \theta$, so that the displacement thickness on the cone is

$$\delta^* = (1 + 0.277M_2^2)\left(\frac{\nu_2 \xi \sec \theta}{u_2}\right)^{1/2} \tag{B4}$$

Substituting equation (B4) into equation (B1),

$$r = a\xi + b\xi^{1/2} \tag{B5}$$

where

$$a = \tan \theta$$

$$b = \sec^{3/2}\theta(1 + 0.277M_2^2)\left(\frac{\nu_2}{u_2}\right)^{1/2}$$

Thus the cross-sectional area of the "effective body" is

$$S = \pi\left(a\xi + b\xi^{1/2}\right)^2 \tag{B6}$$

Let p_2 be the pressure at the surface of the cone and define a surface pressure coefficient C_p as

$$C_p = \frac{p_2 - p_1}{\frac{1}{2}\rho_1 u_1^2} \tag{B7}$$

where the subscript 1 refers to the undisturbed free stream. In reference 24 this pressure coefficient is related to the body geometry and the free-stream Mach number M_1 by a first-order solution of the linearized equations of supersonic flow about uniformly continuous bodies of revolution. The result is

$$C_p = \frac{1}{\pi}\left[\frac{S'}{\xi} - \left(1 + \log_e \frac{r\sqrt{M_1^2 - 1}}{2\xi}\right)S'' - \frac{\xi}{2}S''' + \frac{\xi^2}{12}S^{iv} - \frac{\xi^3}{72}S^{v} + \frac{\xi^4}{480}S^{vi} + \ldots\right] - (r')^2 + O(r^3) \tag{B8}$$

where primes and Roman numeral superscripts denote differentiation with respect to ξ. It is pointed out further in reference 24 that, for the case of an infinite slender body of revolution, the rigorous first-order linearized solution is

$$C_p \approx -\frac{S''}{\pi} \log_e \left(\frac{r}{\xi}\right) \quad \text{for} \quad M_1 \approx \sqrt{2} \tag{B9}$$

Substituting equations (B5) and (B6) into equation (B9),

$$C_p \approx -2\left(a^2 + \frac{3ab}{4} \xi^{-1/2}\right) \log_e \left(a + b\xi^{-1/2}\right) \tag{B10}$$

For cones of small angle, the approximations $\tan \theta \approx \theta$ and $\sec \theta \approx 1$ are made, whereby

$$\left.\begin{aligned} a &\approx \theta \\ b &\approx \left(1 + 0.277M_2^2\right)\left(\frac{\nu_2}{u_2}\right)^{1/2} \end{aligned}\right\} \tag{B11}$$

Then

$$C_p \approx -2\left\{\theta^2 + \frac{3\theta}{4}\left[\frac{1 + 0.277M_2^2}{\sqrt{(Re_x)_2}}\right]\right\} \log_e \left[\theta + \frac{1 + 0.277M_2^2}{\sqrt{(Re_x)_2}}\right] \tag{B12}$$

where $(Re_x)_2 = u_2 x/\nu_2$. This expression may be simplified by expanding the logarithmic term and dropping all terms containing $\left[(Re_x)_2\right]^{-n}$, $n > \frac{1}{2}$, since terms of these higher orders are neglected in all boundary-layer theory. One obtains

$$C_p \approx 2\theta^2 \log_e \left(\frac{1}{\theta}\right) + \left[\frac{3}{2}\theta \log_e \left(\frac{1}{\theta}\right) - 2\theta\right] \frac{1 + 0.277M_2^2}{\sqrt{(Re_x)_2}} \tag{B13}$$

To a consistent degree of approximation in the linearized nonviscous flow, M_2 is related to M_1 and θ by

$$M_2^2 \approx M_1^2\left[1 + \theta^2(1 + 2 \log_e \theta)\right] \tag{B14}$$

Note that for vanishing viscosity, $(Re_x)_2 \longrightarrow \infty$, one obtains from equation (B13) the result

$$C_p \approx 2\theta^2 \log_e \left(\frac{1}{\theta}\right) \tag{B15}$$

RESULTS

For wind-tunnel applications the quantity $\frac{p_2}{p_{2i}} - 1$ is of interest. From the perfect-gas law and the defining relation for the speed of sound

$$\rho u^2 = \gamma p M^2 \tag{B16}$$

One obtains for the pressure ratio

$$\frac{p_2}{p_{2i}} = \frac{1 + \frac{\gamma}{2} M_1^2 C_p}{1 + \frac{\gamma}{2} M_1^2 C_{pi}} \tag{B17}$$

and, substituting from equations (B13), (B14), and (B15) and defining a second pressure coefficient,

$$C_p' = \frac{p_2}{p_{2i}} - 1 = \frac{f(M_1,\theta)}{\sqrt{(Re_x)_2}} \tag{B18}$$

where

$$f(M_1,\theta) = \frac{\gamma}{4} M_1^2\left[3\theta \log_e \left(\frac{1}{\theta}\right) - 4\theta\right]\left(1 + 0.277M_1^2\left\{1 - \theta^2\left[2 \log_e \left(\frac{1}{\theta}\right) - 1\right]\right\}\right) \tag{B19}$$

The quantity $f(M_1,\theta)$ is plotted versus M_1 in figure 11 for $\theta = 5^\circ$, 7.5°, and 10°.

DISCUSSION

Equation (B19) shows that the viscous boundary layer on the surface of an infinite cone at zero angle of attack in a uniform supersonic stream causes an increase in the surface pressure on the cone. This pressure increase is dependent on the distance from the cone vertex.

Roughly speaking, the actual surface pressure will differ appreciably (say by 1 percent or more) from the ideal surface pressure when the local Reynolds number of the flow at the boundary-layer seam is less than 10^5, the difference increasing in proportion to $1/\sqrt{(Re_x)_2}$ as $(Re_x)_2$ decreases. For free-stream Mach numbers greater than 2.5 the theoretically calculated pressure coefficient C_p' is sensitive to variations in M_1 and θ.

The limitations of the foregoing analysis are severe and should be recognized in some detail. By the nature of its basic assumptions, boundary-layer theory is applicable only when viscous layers are reasonably thin compared with the distance from the vertex and the radius of the body. It can be shown from equations (B1) and (B4) that

$$\frac{\delta^*}{r_o} = \frac{1 + 0.277M_2^2}{\sqrt{(Re_x)_2}\sin\theta}$$

where r_o is the radius of the body without δ^* added. For $\theta = 5^\circ$ and $M_2 = 4$, $\delta^*/r_o \approx 50/\sqrt{(Re_x)_2}$ so that for δ^* to be small compared with r_o (say less than 15 percent of r_o) the Reynolds number $(Re_x)_2$ must be greater than 10^5. Consequently, the results of the present analysis should be numerically significant only in the range of Reynolds number $10^5 < (Re_x)_2 < 10^6$ and serve only to indicate qualitative trends for lower values of $(Re_x)_2$. Similarly, linearized theory is best when restricted to very slender bodies and moderately low Mach numbers.

Such physical approximations as taking the Prandtl number as unity and μ proportional to T are not serious with respect to theoretical trends, but will have considerable effect on numerical results.

REFERENCES

1. Kane, E. D., and Maslach, G. J.: Impact-Pressure Interpretation in a Rarefied Gas at Supersonic Speeds. NACA TN 2210, 1950.

2. Kane, E. D., and Schaaf, S. A.: Viscous Effects on Impact Probes in a Subsonic Rarefied Gas Flow. Rep. No. HE-150-82, Contract NAw-5754, NACA and Univ. of Calif., Mar. 9, 1951.

3. Chambré, P. L., and Smith, H. R.: The Impact Tube in a Viscous Compressible Gas. Rep. No. HE-150-63, Contract No. N7-ONR-295-Task 3, Office of Naval Res. and Eng. Res. Projects, Univ. of Calif., Aug. 29, 1949. (Also Heat Transfer and Fluid Mechanics Institute June 1949, Berkeley, Calif., A.S.M.E., 1949, pp. 271-278.)

4. Chambré, P. L.: The Theory of the Impact Tube in a Viscous Compressible Gas. Rep. No. HE-150-50, Contract No. N7-ONR-295-Task 3, Office of Naval Res. and Eng. Res. Projects, Univ. of Calif., Nov. 1, 1948.

5. Lin, T. C., and Schaaf, S. A.: Effect of Slip on Flow Near a Stagnation Point and in a Boundary Layer. NACA TN 2568, 1951.

6. Ipsen, D. C.: Viscosity Correction to Impact Pressure on Prolate Spheroid. Rep. No. HE-150-89, Contract No. N7-ONR-295-Task 3, Office of Naval Res., Air Res. and Dev. Command, and Inst. Eng. Res., Univ. of Calif., Mar. 12, 1952.

7. Sherman, F. S.: New Experiments on Impact-Pressure Interpretation in Supersonic and Subsonic Rarefied Air Streams. NACA TN 2995, 1953.

8. Schaaf, S. A., Horning, Don O., and Kane, E. D.: Design and Initial Operation of a Low Density Supersonic Wind Tunnel. Rep. No. HE-150-62, Contract N7-ONR-295-Task 3, Office of Naval Res. and Eng. Res. Projects, Univ. of CAlif., Aug. 15, 1949.

9. Emerson, D. E., and Schaaf, S. A.: Performance of a Supersonic Nozzle in the Rarefied Gas Dynamics Regime. Rep. No. HE-150-72, Contract No. N7-ONR-295-Task 3, Office of Naval Res. and Eng. Res. Projects, Univ. of Calif., Aug. 30, 1950.

10. Owen, J. M., and Sherman, F. S.: Design and Testing of a Mach 4 Axially Symmetric Nozzle for Rarefied Gas Flows. Rep. No. HE-150-104, Contract No. N7-ONR-295, Office of Naval Res., Office of Sci. Res., and Inst. Eng. Res., Univ. of Calif., July 23, 1952.

11. Maslach, G. J.: A Precision Manometer for Low Pressures. Rep. No. HE-150-75, Contract No. N7-onr-295-Task 3, Office of Naval Res. and Inst. Eng. Res., Univ. of Calif., Oct. 27, 1950.

12. Anon.: Handbook of Supersonic Aerodynamics. NAVORD Rep. 1488, vol. 2, sec. 5, Bur. Ord., Dept. Navy, and Appl. Phys. Lab., The Johns Hopkins Univ., Oct. 1, 1950.

13. Ackeret, J., Feldmann, F., and Rott, N.: Investigations of Compression Shocks and Boundary Layers in Gases Moving at High Speed. NACA TM 1113, 1947.

14. Lee, J. D.: The Influence of High Adverse Pressure Gradients on Boundary Layers in Supersonic Flow. Rep. No. 21, Inst. Aerophys., Univ. of Toronto, Oct. 1952.

15. Kennard, Earle H.: Kinetic Theory of Gases. First ed., McGraw-Hill Book Co., Inc., 1938, pp. 331-332.

16. Drake, R. M., Jr., and Maslach, G. J.: Heat Transfer From Right Circular Cones to a Rarefied Gas in Supersonic Flow. Rep. HE-150-91, Contract N7-ONR-295, Office of Naval Res., Office of Sci. Res., and Inst. Eng. Res., Univ. of Calif., Apr. 8, 1952.

17. Van Dyke, Milton D.: A Study of Second-Order Supersonic-Flow Theory. NACA Rep. 1081, 1952. (Supersedes NACA TN 2200.)

18. Ehret, Dorris M.: Accuracy of Approximate Methods for Predicting Pressures on Pointed Nonlifting Bodies of Revolution in Supersonic Flow. NACA TN 2764, 1952.

19. Taylor, G. I., and Maccoll, J. W.: The Air Pressure Over a Cone Moving at High Speeds. Proc. Roy. Soc. (London), ser. A, vol. 139, No. 838, Feb. 1, 1933, pp. 278-311.

20. Staff of the Computing Section (under the direction of Zdenek Kopal): Tables of Supersonic Flow Around Cones. Tech. Rep. No. 1, Center of Analysis, M.I.T., 1947.

21. Lin, T. C., Schaaf, S. A., and Sherman, F. S.: Boundary Layer Effect on the Surface Pressure of an Infinite Cone in Supersonic Flow. Rep. No. HE-150-80, Contract NAw-6004, NACA and Univ. of Calif., Mar. 5, 1951.

22. Hantzsche, W., and Wendt, H.: Die laminare Grenzschicht bei einem mit Überschallgeschwindigkeit angestroemten nichtangestellten Kreiskegel. Jahrbuch 1941, deutschen Luftfahrtforschung, pp. I 76 - I 77.

23. Howarth, L.: Concerning the Effect of Compressibility on Laminar Boundary Layers and Their Separation. Proc. Roy. Soc. (London), ser. A, vol. 194, no. 1036, July 28, 1948, pp. 16-42.

24. Laitone, E. V.: The Linearized Subsonic and Supersonic Flow About Inclined Slender Bodies of Revolution. Jour. Aero. Sci., vol. 14, no. 11, Nov. 1947, pp. 631-642.

TABLE I

MACH NUMBER, p_{1ti}'/p_{2i}, AND p_{2i}/p_1 FOR 5° SEMIVERTEX-ANGLE CONE

M_1	p_{1ti}'/p_{2i}	p_{2i}/p_1	M_1	p_{1ti}'/p_{2i}	p_{2i}/p_1	M_1	p_{1ti}'/p_{2i}	p_{2i}/p_1	M_1	p_{1ti}'/p_{2i}	p_{2i}/p_1
1.00			1.60	3.57	1.068	2.20	6.05	1.110	2.80	9.10	1.160
1.01			1.61	3.61	1.069	2.21	6.10	1.111	2.81	9.16	1.161
1.02			1.62	3.64	1.070	2.22	6.15	1.112	2.82	9.21	1.162
1.03			1.63	3.68	1.070	2.23	6.19	1.112	2.83	9.27	1.163
1.04			1.64	3.72	1.071	2.24	6.24	1.113	2.84	9.32	1.164
1.05			1.65	3.75	1.072	2.25	6.29	1.114	2.85	9.38	1.164
1.06			1.66	3.79	1.072	2.26	6.33	1.115	2.86	9.43	1.165
1.07			1.67	3.83	1.073	2.27	6.38	1.116	2.87	9.48	1.166
1.08			1.68	3.87	1.074	2.28	6.43	1.116	2.88	9.54	1.167
1.09			1.69	3.91	1.074	2.29	6.47	1.117	2.89	9.59	1.168
1.10	2.05	1.045	1.70	3.94	1.075	2.30	6.52	1.118	2.90	9.65	1.169
1.11	2.07	1.045	1.71	3.98	1.076	2.31	6.57	1.119	2.91	9.71	1.170
1.12	2.09	1.045	1.72	4.02	1.076	2.32	6.62	1.120	2.92	9.76	1.171
1.13	2.11	1.045	1.73	4.06	1.077	2.33	6.66	1.120	2.93	9.82	1.172
1.14	2.13	1.046	1.74	4.09	1.078	2.34	6.71	1.121	2.94	9.88	1.173
1.15	2.15	1.046	1.75	4.13	1.078	2.35	6.76	1.122	2.95	9.93	1.173
1.16	2.18	1.046	1.76	4.17	1.079	2.36	6.81	1.123	2.96	9.99	1.174
1.17	2.21	1.047	1.77	4.21	1.080	2.37	6.85	1.124	2.97	10.04	1.175
1.18	2.24	1.047	1.78	4.25	1.080	2.38	6.90	1.124	2.98	10.10	1.176
1.19	2.27	1.047	1.79	4.28	1.081	2.39	6.95	1.125	2.99	10.16	1.177
1.20	2.30	1.048	1.80	4.32	1.082	2.40	7.00	1.126	3.00	10.21	1.178
1.21	2.32	1.048	1.81	4.36	1.082	2.41	7.05	1.127	3.01	10.27	1.179
1.22	2.35	1.048	1.82	4.40	1.083	2.42	7.10	1.128	3.02	10.33	1.180
1.23	2.37	1.049	1.83	4.44	1.084	2.43	7.16	1.128	3.03	10.39	1.181
1.24	2.40	1.049	1.84	4.48	1.085	2.44	7.21	1.129	3.04	10.45	1.182
1.25	2.43	1.050	1.85	4.52	1.085	2.45	7.26	1.130	3.05	10.51	1.183
1.26	2.46	1.050	1.86	4.56	1.086	2.46	7.31	1.131	3.06	10.57	1.184
1.27	2.49	1.050	1.87	4.60	1.087	2.47	7.36	1.132	3.07	10.63	1.185
1.28	2.52	1.051	1.88	4.64	1.088	2.48	7.42	1.132	3.08	10.69	1.186
1.29	2.55	1.051	1.89	4.68	1.089	2.49	7.47	1.133	3.09	10.75	1.187
1.30	2.58	1.052	1.90	4.72	1.089	2.50	7.52	1.134	3.10	10.81	1.188
1.31	2.61	1.052	1.91	4.76	1.090	2.51	7.57	1.135	3.11	10.87	1.189
1.32	2.64	1.053	1.92	4.80	1.090	2.52	7.62	1.136	3.12	10.93	1.190
1.33	2.67	1.053	1.93	4.85	1.091	2.53	7.68	1.136	3.13	10.99	1.191
1.34	2.70	1.054	1.94	4.89	1.092	2.54	7.73	1.137	3.14	11.05	1.192
1.35	2.73	1.054	1.95	4.93	1.093	2.55	7.78	1.138	3.15	11.11	1.193
1.36	2.76	1.055	1.96	4.97	1.093	2.56	7.83	1.139	3.16	11.17	1.194
1.37	2.80	1.055	1.97	5.02	1.094	2.57	7.88	1.140	3.17	11.23	1.195
1.38	2.83	1.056	1.98	5.06	1.095	2.58	7.94	1.140	3.18	11.29	1.196
1.39	2.86	1.056	1.99	5.10	1.096	2.59	7.99	1.141	3.19	11.35	1.197
1.40	2.90	1.057	2.00	5.15	1.096	2.60	8.04	1.142	3.20	11.41	1.198
1.41	2.93	1.057	2.01	5.19	1.097	2.61	8.09	1.143	3.21	11.47	1.199
1.42	2.96	1.058	2.02	5.24	1.097	2.62	8.15	1.144	3.22	11.53	1.200
1.43	3.00	1.058	2.03	5.29	1.098	2.63	8.20	1.145	3.23	11.59	1.201
1.44	3.03	1.059	2.04	5.33	1.099	2.64	8.25	1.146	3.24	11.65	1.202
1.45	3.06	1.059	2.05	5.38	1.100	2.65	8.31	1.146	3.25	11.71	1.203
1.46	3.10	1.060	2.06	5.42	1.100	2.66	8.36	1.147	3.26	11.78	1.204
1.47	3.13	1.060	2.07	5.47	1.101	2.67	8.41	1.148	3.27	11.84	1.205
1.48	3.16	1.061	2.08	5.51	1.102	2.68	8.47	1.149	3.28	11.90	1.206
1.48	3.20	1.061	2.09	5.56	1.102	2.69	8.52	1.150	3.29	11.96	1.207
1.50	3.23	1.062	2.10	5.60	1.103	2.70	8.57	1.151	3.30	12.02	1.208
1.51	3.26	1.063	2.11	5.65	1.104	2.71	8.62	1.152	3.31	12.08	1.209
1.52	3.29	1.064	2.12	5.69	1.104	2.72	8.67	1.153	3.32	12.14	1.210
1.53	3.33	1.064	2.13	5.74	1.105	2.73	8.73	1.154	3.33	12.20	1.211
1.54	3.36	1.065	2.14	5.78	1.106	2.74	8.78	1.155	3.34	12.26	1.212
1.55	3.39	1.065	2.15	5.83	1.107	2.75	8.84	1.155	3.35	12.33	1.213
1.56	3.43	1.066	2.16	5.87	1.107	2.76	8.89	1.156	3.36	12.39	1.214
1.57	3.46	1.067	2.17	5.92	1.108	2.77	8.94	1.157	3.37	12.45	1.215
1.58	3.50	1.067	2.18	5.96	1.109	2.78	9.00	1.158	3.38	12.51	1.216
1.59	3.54	1.068	2.19	6.00	1.109	2.79	9.05	1.159	3.39	12.57	1.217

TABLE I.- Concluded

MACH NUMBER, p_{1t1}'/p_{21}, AND p_{21}/p_1 FOR 5° SEMIVERTEX-ANGLE CONE

M_1	p_{1t1}'/p_{21}	p_{21}/p_1	M_1	p_{1t1}'/p_{21}	p_{21}/p_1	M_1	p_{1t1}'/p_{21}	p_{21}/p_1	M_1	p_{1t1}'/p_{21}	p_{21}/p_1
3.40	12.63	1.218	4.05	16.78	1.287	4.70	21.20	1.365	5.35	25.70	1.453
3.41	12.69	1.219	4.06	16.84	1.288	4.71	21.27	1.366	5.36	25.76	1.455
3.42	12.75	1.220	4.07	16.91	1.290	4.72	21.34	1.368	5.37	25.83	1.456
3.43	12.81	1.221	4.08	16.98	1.291	4.73	21.41	1.369	5.38	25.90	1.458
3.44	12.87	1.222	4.09	17.05	1.292	4.74	21.48	1.370	5.39	25.97	1.459
3.45	12.94	1.223	4.10	17.11	1.293	4.75	21.54	1.371	5.40	26.04	1.460
3.46	13.00	1.224	4.11	17.18	1.294	4.76	21.61	1.373	5.41	26.11	1.462
3.47	13.06	1.225	4.12	17.25	1.295	4.77	21.68	1.374	5.42	26.18	1.463
3.48	13.12	1.226	4.13	17.31	1.296	4.78	21.75	1.375	5.43	26.25	1.465
3.49	13.18	1.227	4.14	17.38	1.297	4.79	21.82	1.377	5.44	26.32	1.466
3.50	13.24	1.228	4.15	17.45	1.298	4.80	21.88	1.378	5.45	26.39	1.467
3.51	13.30	1.229	4.16	17.51	1.299	4.81	21.95	1.379	5.46	26.46	1.469
3.52	13.36	1.230	4.17	17.58	1.300	4.82	22.02	1.380	5.47	26.53	1.470
3.53	13.42	1.232	4.18	17.65	1.302	4.83	22.09	1.382	5.48	26.60	1.472
3.54	13.48	1.233	4.19	17.72	1.303	4.84	22.16	1.383	5.49	26.67	1.473
3.55	13.55	1.234	4.20	17.78	1.304	4.85	22.23	1.384	5.50	26.74	1.474
3.56	13.61	1.235	4.21	17.85	1.305	4.86	22.30	1.385	5.51	26.80	1.476
3.57	13.67	1.236	4.22	17.91	1.307	4.87	22.37	1.387	5.52	26.87	1.477
3.58	13.73	1.237	4.23	17.98	1.308	4.88	22.44	1.388	5.53	26.94	1.479
3.59	13.79	1.238	4.24	18.05	1.309	4.89	22.51	1.390	5.54	27.01	1.480
3.60	13.85	1.239	4.25	18.11	1.310	4.90	22.58	1.391	5.55	27.08	1.481
3.61	13.91	1.240	4.26	18.18	1.311	4.91	22.65	1.392	5.56	27.15	1.483
3.62	13.97	1.241	4.27	18.25	1.313	4.92	22.72	1.394	5.57	27.22	1.484
3.63	14.04	1.242	4.28	18.32	1.314	4.93	22.79	1.395	5.58	27.29	1.486
3.64	14.10	1.243	4.29	18.39	1.315	4.94	22.86	1.397	5.59	27.36	1.487
3.65	14.16	1.244	4.30	18.45	1.316	4.95	22.93	1.398	5.60	27.43	1.488
3.66	14.22	1.245	4.31	18.52	1.317	4.96	23.00	1.399	5.61	27.50	1.490
3.67	14.29	1.246	4.32	18.59	1.318	4.97	23.07	1.400	5.62	27.57	1.491
3.68	14.35	1.247	4.33	18.66	1.320	4.98	23.14	1.402	5.63	27.64	1.493
3.69	14.41	1.248	4.34	18.72	1.321	4.99	23.21	1.403	5.64	27.71	1.494
3.70	14.47	1.249	4.35	18.79	1.322	5.00	23.28	1.405	5.65	27.77	1.495
3.71	14.54	1.250	4.36	18.86	1.323	5.01	23.34	1.406	5.66	27.84	1.497
3.72	14.60	1.251	4.37	18.93	1.325	5.02	23.41	1.408	5.67	27.91	1.498
3.73	14.66	1.252	4.38	19.00	1.326	5.03	23.48	1.409	5.68	27.98	1.500
3.74	14.72	1.253	4.39	19.07	1.327	5.04	23.55	1.410	5.69	28.05	1.502
3.75	14.79	1.255	4.40	19.13	1.328	5.05	23.62	1.411	5.70	28.12	1.503
3.76	14.85	1.256	4.41	19.19	1.329	5.06	23.69	1.413	5.71	28.19	1.505
3.77	14.91	1.257	4.42	19.26	1.331	5.07	23.76	1.414	5.72	28.26	1.506
3.78	14.98	1.258	4.43	19.33	1.332	5.08	23.83	1.416	5.73	28.33	1.508
3.79	15.04	1.259	4.44	19.40	1.333	5.09	23.90	1.417	5.74	28.40	1.509
3.80	15.10	1.260	4.45	19.47	1.334	5.10	23.97	1.418	5.75	28.47	1.510
3.81	15.16	1.261	4.46	19.54	1.335	5.11	24.04	1.420	5.76	28.53	1.512
3.82	15.23	1.262	4.47	19.61	1.337	5.12	24.11	1.421	5.77	28.60	1.513
3.83	15.29	1.263	4.48	19.68	1.338	5.13	24.18	1.423	5.78	28.67	1.515
3.84	15.36	1.264	4.49	19.75	1.339	5.14	24.25	1.424	5.79	28.74	1.516
3.85	15.42	1.266	4.50	19.81	1.340	5.15	24.32	1.425	5.80	28.81	1.517
3.86	15.49	1.267	4.51	19.88	1.341	5.16	24.39	1.427	5.81	28.88	1.519
3.87	15.55	1.268	4.52	19.95	1.343	5.17	24.45	1.428	5.82	28.95	1.520
3.88	15.62	1.269	4.53	20.02	1.344	5.18	24.52	1.430	5.83	29.02	1.522
3.89	15.68	1.270	4.54	20.09	1.345	5.19	24.59	1.431	5.84	29.09	1.524
3.90	15.74	1.271	4.55	20.16	1.346	5.20	24.66	1.432	5.85	29.16	1.525
3.91	15.80	1.272	4.56	20.23	1.347	5.21	24.73	1.434	5.86	29.22	1.527
3.92	15.87	1.273	4.57	20.29	1.349	5.22	24.80	1.435	5.87	29.29	1.528
3.93	15.93	1.274	4.58	20.36	1.350	5.23	24.87	1.437	5.88	29.36	1.529
3.94	16.00	1.275	4.59	20.43	1.351	5.24	24.94	1.438	5.89	29.43	1.531
3.95	16.06	1.277	4.60	20.50	1.352	5.25	25.01	1.439	5.90	29.50	1.532
3.96	16.13	1.278	4.61	20.57	1.353	5.26	25.07	1.441	5.91	29.57	1.534
3.97	16.19	1.279	4.62	20.64	1.355	5.27	25.14	1.442	5.92	29.64	1.535
3.98	16.26	1.280	4.63	20.71	1.356	5.28	25.21	1.443	5.93	29.71	1.536
3.99	16.32	1.281	4.64	20.78	1.358	5.29	25.28	1.445	5.94	29.78	1.538
4.00	16.44	1.281	4.65	20.85	1.359	5.30	25.35	1.446	5.95	29.85	1.539
4.01	16.51	1.282	4.66	20.92	1.360	5.31	25.42	1.448	5.96	29.92	1.541
4.02	16.58	1.284	4.67	20.99	1.362	5.32	25.49	1.449	5.97	29.99	1.542
4.03	16.64	1.285	4.68	21.06	1.363	5.33	25.56	1.451	5.98	30.06	1.544
4.04	16.71	1.286	4.69	21.13	1.364	5.34	25.63	1.452	5.99	30.13	1.545

TABLE II

PRESSURE COEFFICIENTS FOR TYPE A CONES

[Nozzle 8]

Flow, lb/hr	Model	M_1	p_1, μ Hg	p_2, μ Hg	p_{21}, μ Hg	C_p'	x, in.	$\frac{1}{\sqrt{(Re_x)_1}}$	$f(M_1,\theta)$
5.2	A1	3.70	50.6	90.3	63.2	0.428	0.20	0.0734	4.798
	A2			86.3		.365	.30	.0599	
	A3			82.1		.299	.40	.0519	
	A4			80.3		.270	.50	.0464	
	A5			77.4		.224	.75	.0379	
	A6			76.4		.209	1.00	.0328	
	A7			75.1		.188	1.50	.0268	
10.3	A1	3.89	74.2	127.1	94.2	.349	.20	.0556	5.583
	A2			124.7		.323	.30	.0454	
	A3			118.2		.254	.40	.0393	
	A4			115.5		.226	.50	.0352	
	A5			112.7		.196	.75	.0287	
	A6			111.0		.178	1.00	.0249	
	A7			108.9		.156	1.50	.0203	
14.8	A1	3.95	90.4	151.3	115.5	.310	.20	.0490	5.858
	A2			148.2		.283	.30	.0400	
	A3			142.0		.229	.40	.0346	
	A4			138.6		.200	.50	.0309	
	A5			135.4		.172	.75	.0253	
	A6			133.0		.152	1.00	.0219	
	A7			130.4		.129	1.50	.0179	
20	A1	4.07	111.4	191.0	143.5	.331	.20	.0420	6.381
	A2			189.7		.322	.30	.0343	
	A3			180.3		.256	.40	.0297	
	A4			174.7		.217	.50	.0266	
	A5			171.0		.192	.75	.0217	
	A6			167.7		.169	1.00	.0188	
	A7			165.8		.142	1.50	.0153	
26	A1	4.13	134.3	229.3	174.1	.317	.20	.0372	6.685
	A2			226.9		.303	.30	.0304	
	A3			218.1		.253	.40	.0263	
	A4			211.2		.213	.50	.0235	
	A5			207.2		.190	.75	.0192	
	A6			203.3		.168	1.00	.0166	
	A7			198.4		.140	1.50	.0136	
5.2	A8	3.68	51.1	73.8	63.7	.158	1.94	.0236	4.712
	A9			73.8		.158	2.42	.0212	
	A10			71.9		.128	2.94	.0192	
	A11			71.9		.128	3.28	.0182	
	A12			70.9		.112	3.32	.0181	
	A13			67.9		.066	3.41	.0178	
	A14			59.1		-.073	----	------	
10.3	A8	3.91	73.0	107.2	92.9	.154	1.94	.0178	5.671
	A9			107.2		.154	2.42	.0160	
	A10			105.2		.133	2.94	.0145	
	A11			103.3		.112	3.28	.0137	
	A12			103.3		.112	3.32	.0136	
	A13			97.4		.049	3.41	.0135	
	A14			85.6		-.078	----	------	
14.8	A8	3.98	89.2	126.8	114.1	.111	1.94	.0157	5.962
	A9			124.8		.094	2.42	.0140	
	A10			122.9		.077	2.94	.0127	
	A11			120.9		.060	3.28	.0120	
	A12			120.9		.060	3.32	.0120	
	A13			117.0		.025	3.41	.0118	
	A14			101.3		-.112	----	------	
20	A8	4.05	113.2	162.2	145.7	.113	1.94	.0135	6.305
	A9			159.3		.093	2.42	.0121	
	A10			155.3		.066	2.94	.0110	
	A11			155.3		.066	3.28	.0104	
	A12			153.3		.052	3.32	.0103	
	A13			145.5		-.001	3.41	.0102	
	A14			125.7		-.137	----	------	
26	A8	4.13	134.8	192.8	174.7	.104	1.94	.0119	6.670
	A9			190.8		.092	2.42	.0107	
	A10			187.8		.075	2.94	.0097	
	A11			185.9		.053	3.28	.0092	
	A12			181.9		.041	3.32	.0091	
	A13			173.1		-.009	3.41	.0090	
	A14			149.4		-.169	----	------	

[a]Cone surface pressures on models A8 to A14 measured with oil manometer.

TABLE III

PRESSURE COEFFICIENTS FOR GEOMETRICALLY SIMILAR CONES (TYPE B)

[Nozzle 8]

Flow, lb/hr	Model	M_1	p_1, μ Hg	p_2, μ Hg	p_{2i}, μ Hg	C_p'	Re_1/in.	x, in.	$\frac{1}{\sqrt{(Re_x)_1}}$
5.2	B1	3.69	50.0	95.5	63.7	0.550	917.6	0.361	0.0550
	B2			84.2		.322		.453	.0490
	B3			80.8		.270		.626	.0417
	B4			80.9		.271		.717	.0390
	B5			82.0		.288		.906	.0347
	B6			78.8		.239		1.167	.0306
	B7			74.6		.171		1.792	.0247
10.3	B1	3.91	72.4	132.6	92.0	.441	1,590	.361	.0418
	B2			121.3		.318		.453	.0373
	B3			117.8		.280		.626	.0317
	B4			118.1		.283		.717	.0296
	B5			118.5		.288		.906	.0264
	B6			116.3		.264		1.167	.0232
	B7			112.0		.217		1.792	.0187
14.8	B1	3.97	88.4	159.6	113.1	.411	2,045	.361	.0368
	B2			146.9		.299		.453	.0329
	B3			142.5		.260		.626	.0280
	B4			143.0		.264		.717	.0261
	B5			142.4		.259		.906	.0232
	B6			140.7		.244		1.167	.0205
	B7			135.5		.198		1.792	.0165
20	B1	4.05	114.2	195.8	147.0	.332	2,831	.361	.0313
	B2			183.3		.247		.453	.0279
	B3			178.6		.215		.626	.0238
	B4			178.9		.217		.717	.0222
	B5			177.0		.204		.906	.0197
	B6			175.9		.197		1.167	.0174
	B7			169.1		.150		1.792	.0140
26	B1	4.12	136.3	230.9	176.5	.308	3,591	.361	.0278
	B2			219.3		.243		.453	.0248
	B3			213.5		.210		.626	.0211
	B4			214.1		.213		.717	.0197
	B5			211.3		.197		.906	.0175
	B6			210.7		.194		1.167	.0155
	B7			203.7		.154		1.792	.0125

TABLE IV

ORIFICE SIZE EFFECT (TYPE C MODELS)

Flow, lb/hr	Model	M_1	Re/in.	d, in.	p_2, μ Hg	p_{2e} (extrapolated to d = 0), μ Hg	Δp_2, μ Hg
Nozzle 6							
5.2	C1	1.95	157.8	0.020	66.8	65.6	1.2
	C2			.040	66.3		.7
	C3			.060	66.1		.5
	C4			.080	66.7		1.1
	C5			.100	66.9		2.3
	C6			.125	67.3		1.7
	C7			.150	69.5		3.9
10.3	C1	2.07	290.0	.020	101.6	101.2	.4
	C2			.040	102.6		1.4
	C3			.060	102.5		1.3
	C4			.080	102.8		1.6
	C5			.100	103.7		2.5
	C6			.125	103.2		2.0
	C7			.150	105.2		4.0
15.5	C1	2.12	418.6	.020	133.8	133.7	.1
	C2			.040	134.7		1.0
	C3			.060	134.8		1.1
	C4			.080	135.1		1.4
	C5			.100	136.4		2.7
	C6			.125	136.0		2.3
	C7			.150	137.7		4.0
20	C1	2.15	514.4	.020	159.9	158.6	.8
	C2			.040	160.1		3.0
	C3			.060	160.0		1.1
	C4			.080	160.5		1.7
	C5			.100	159.6		2.9
	C6			.125	161.1		2.5
	C7			.150	163.7		4.6
26	C1	2.17	665.2	.020	198.1	197.3	.8
	C2			.040	200.3		3.0
	C3			.060	198.4		1.1
	C4			.080	199.0		1.7
	C5			.100	200.2		2.9
	C6			.125	199.8		2.5
	C7			.150	201.9		4.6

TABLE IV.- Concluded

ORIFICE SIZE EFFECT (TYPE C MODELS)

Flow, lb/hr	Model	M_1	Re/in.	d, in.	p_2, μ Hg	p_{2e} (extrapolated to d = 0), μ Hg	Δp_2, μ Hg
Nozzle 6 - Concluded							
30	C1	2.20	762.5	0.020	222.9	222.4	0.5
	C2			.040	224.2		1.8
	C3			.060	224.2		1.8
	C4			.080	224.7		2.3
	C5			.100	226.4		4.0
	C6			.125	225.3		2.9
	C7			.150	226.9		4.5
Nozzle 8							
5.2	C1	3.69	914	0.020	72.8	72.3	0.5
	C2			.040	74.0		1.7
	C3			.060	74.0		1.7
	C4			.080	75.0		2.7
	C5			.100	76.1		3.8
	C6			.125	75.2		2.9
	C7			.150	77.9		5.6
10.3	C1	3.90	1,612	.020	106.9	106.4	.5
	C2			.040	109.5		3.1
	C3			.060	108.5		2.1
	C4			.080	109.5		3.1
	C5			.100	110.8		4.4
	C6			.125	109.5		3.1
	C7			.150	112.0		5.6
14.8	C1	3.96	2,101	.020	128.3	127.9	.4
	C2			.040	129.7		1.8
	C3			.060	129.6		1.7
	C4			.080	130.9		3.0
	C5			.100	132.0		4.1
	C6			.125	130.6		2.7
	C7			.150	132.6		4.7
20	C1	4.02	2,861	.020	158.1	158.1	0
	C2			.040	159.9		1.8
	C3			.060	159.8		1.7
	C4			.080	161.4		3.3
	C5			.100	162.6		4.5
	C6			.125	160.9		2.8
	C7			.150	162.8		4.7

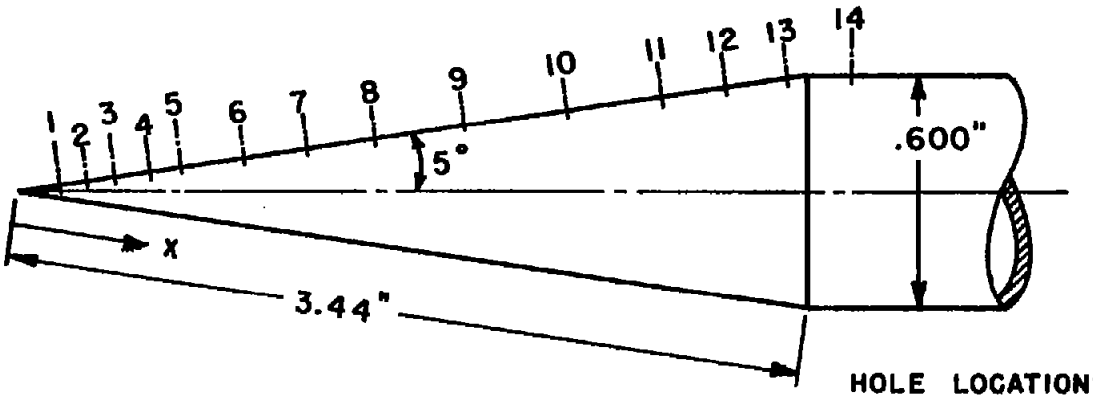

HOLE LOCATIONS
(ALL DISTANCES MEASURED FROM APEX EXCEPT A 14)

MODEL	X, in.	
A 1	0.20	
A 2	.30	
A 3	.40	
A 4	.50	
A 5	.75	
A 6	1.00	
A 7	1.50	
A 8	1.94	
A 9	2.44	
A 10	2.94	
A 11	3.27	
A 12	3.34	
A 13	3.42	
A 14	.30	(FROM SHOULDER)

Figure 1.- Specifications for type A models. 14 cones with 0.600-inch base diameter. Each cone had four pressure orifices of 0.015-inch diameter spaced at 90° intervals around circumference. Cylindrical afterbody $4\frac{1}{2}$ inches long.

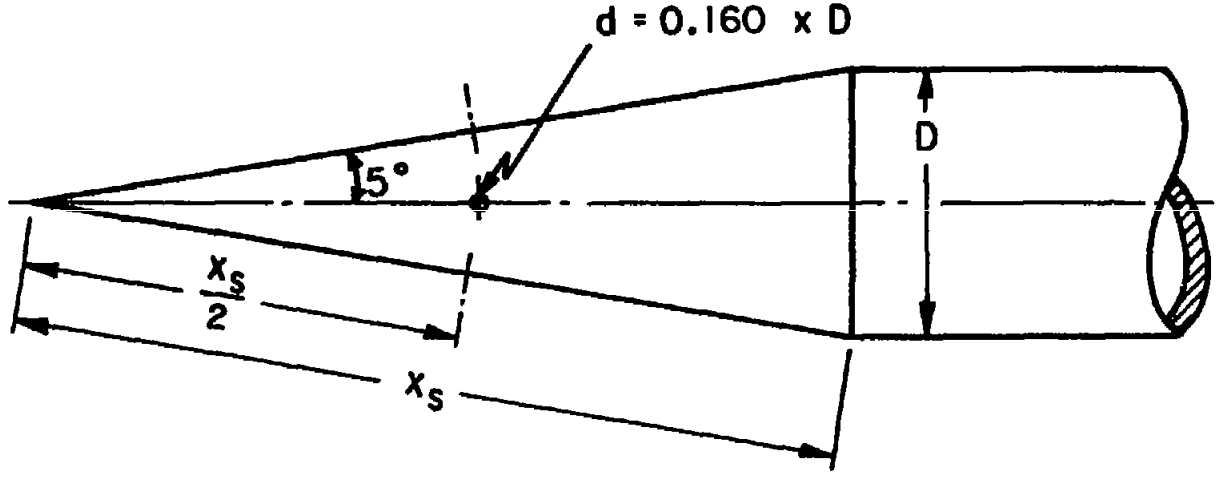

MODEL	D, in.
B 1	0.125
B 2	.158
B 3	.218
B 4	.250
B 5	.316
B 6	.407
B 7	.625

Figure 2.- Specifications for type B models. Seven cones, each with four pressure orifices spaced at 90° intervals around circumference. Cylindrical afterbody 4 inches long.

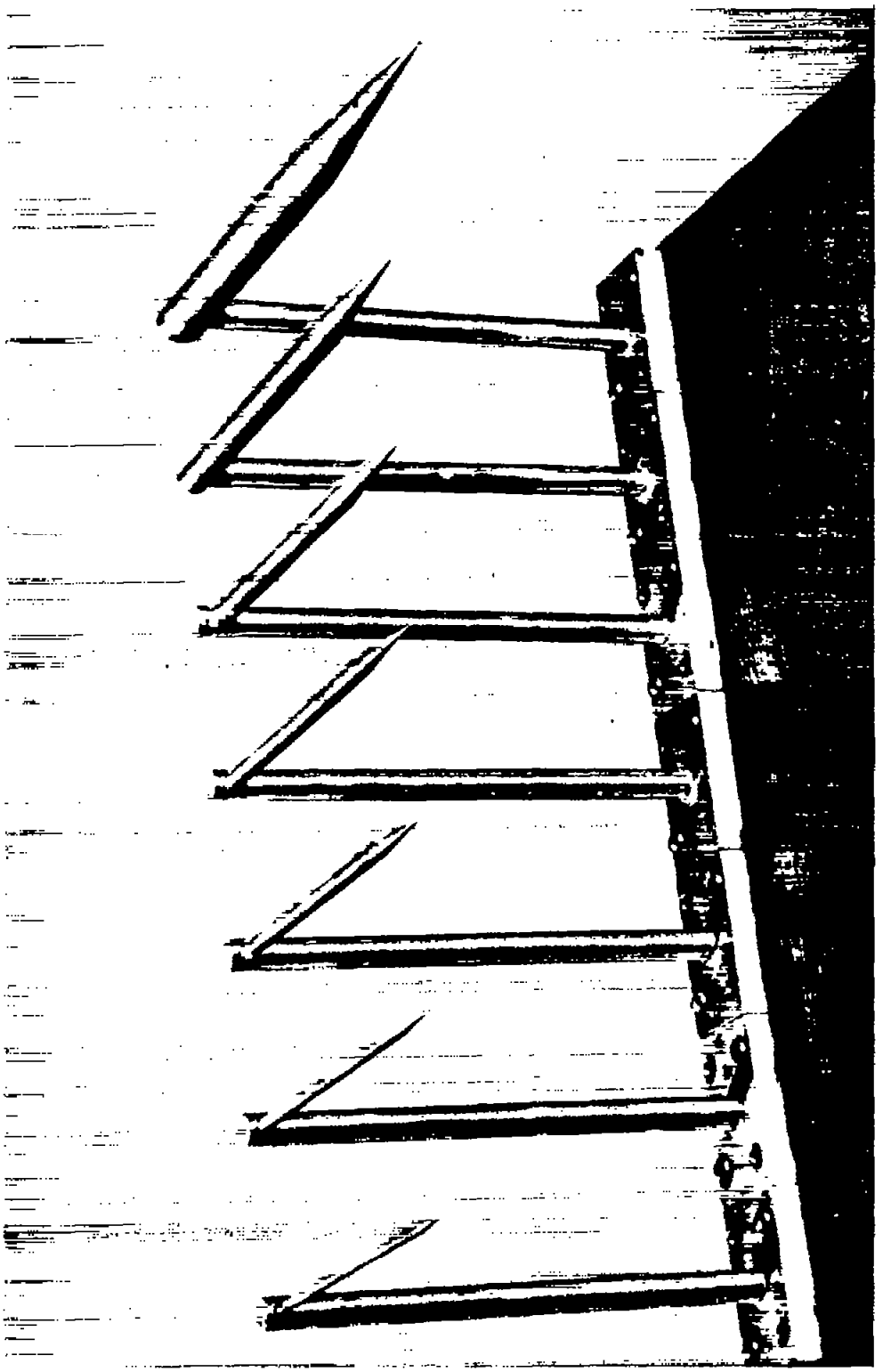

L-85630

Figure 3.- Geometrically similar models (type B).

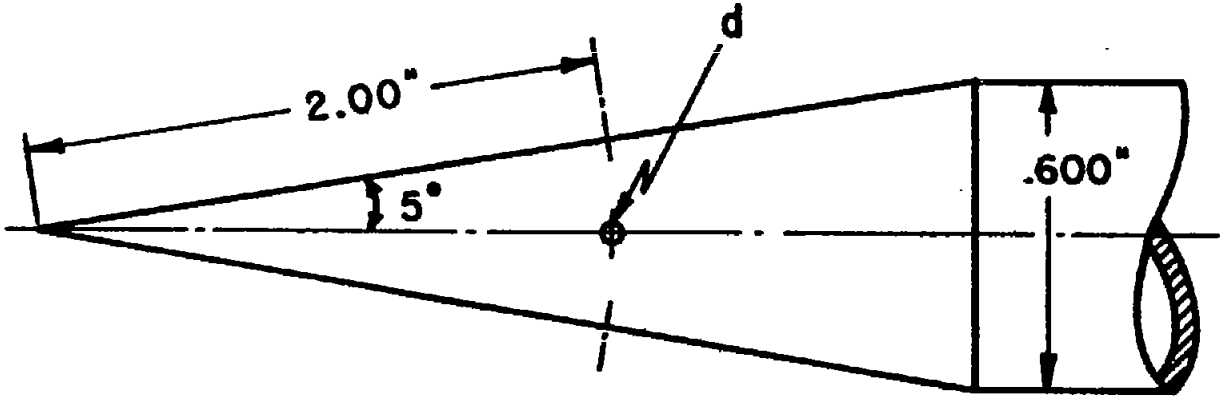

MODEL	d, in.
C 1	0.020
C 2	.040
C 3	.060
C 4	.080
C 5	.100
C 6	.125
C 7	.150

Figure 4.- Specifications for type C models. Seven cones, each of dimensions shown and with four pressure orifices spaced at 90° intervals around circumference. Cylindrical afterbody $4\frac{1}{2}$ inches long.

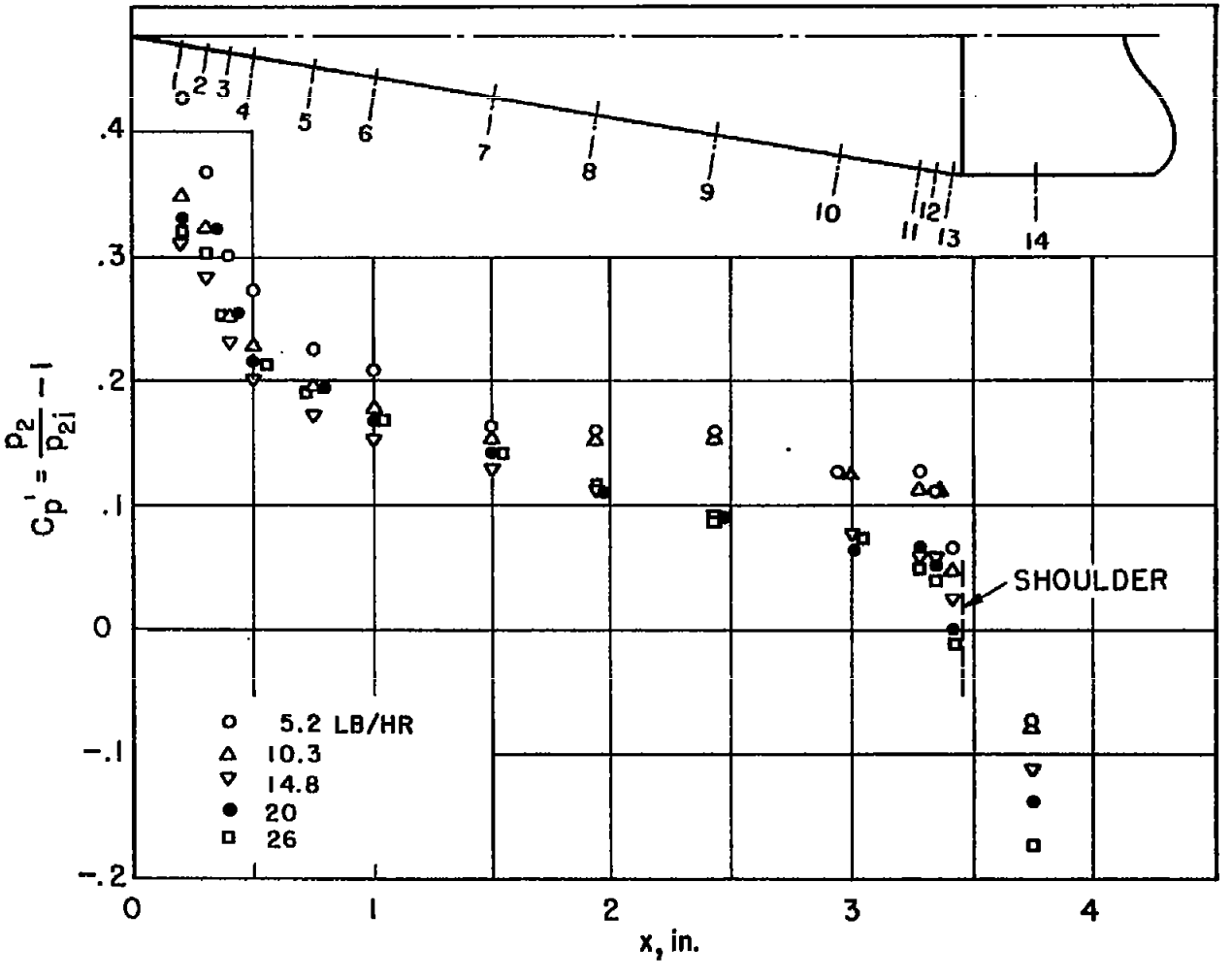

Figure 5.- Cone surface pressure distributions. Type A models. Nozzle 8; $3.70 < M_1 < 4.13$.

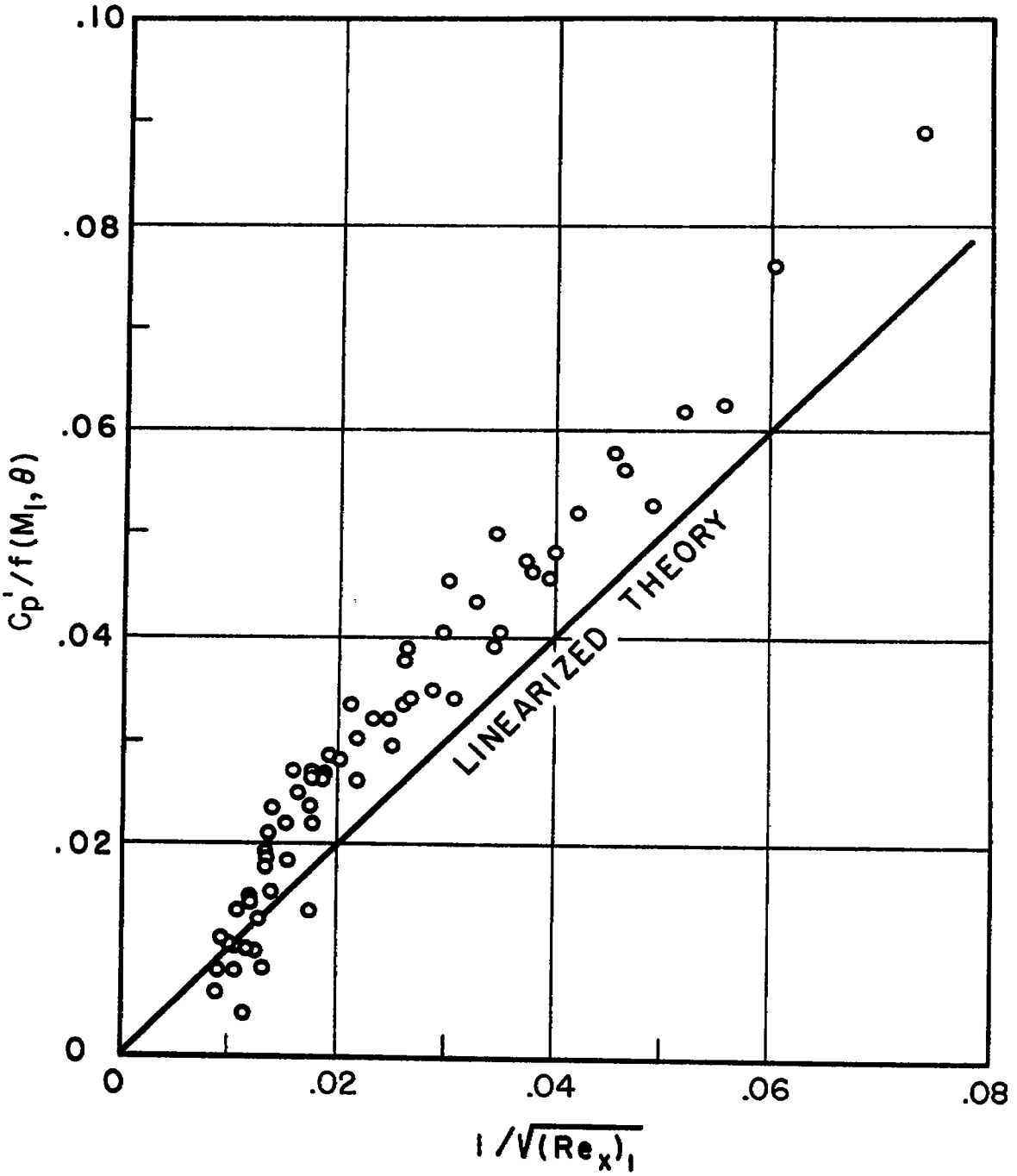

Figure 6.- Comparison between theory and experiment. Type A models. Nozzle 8; $3.70 < M_1 < 4.13$.

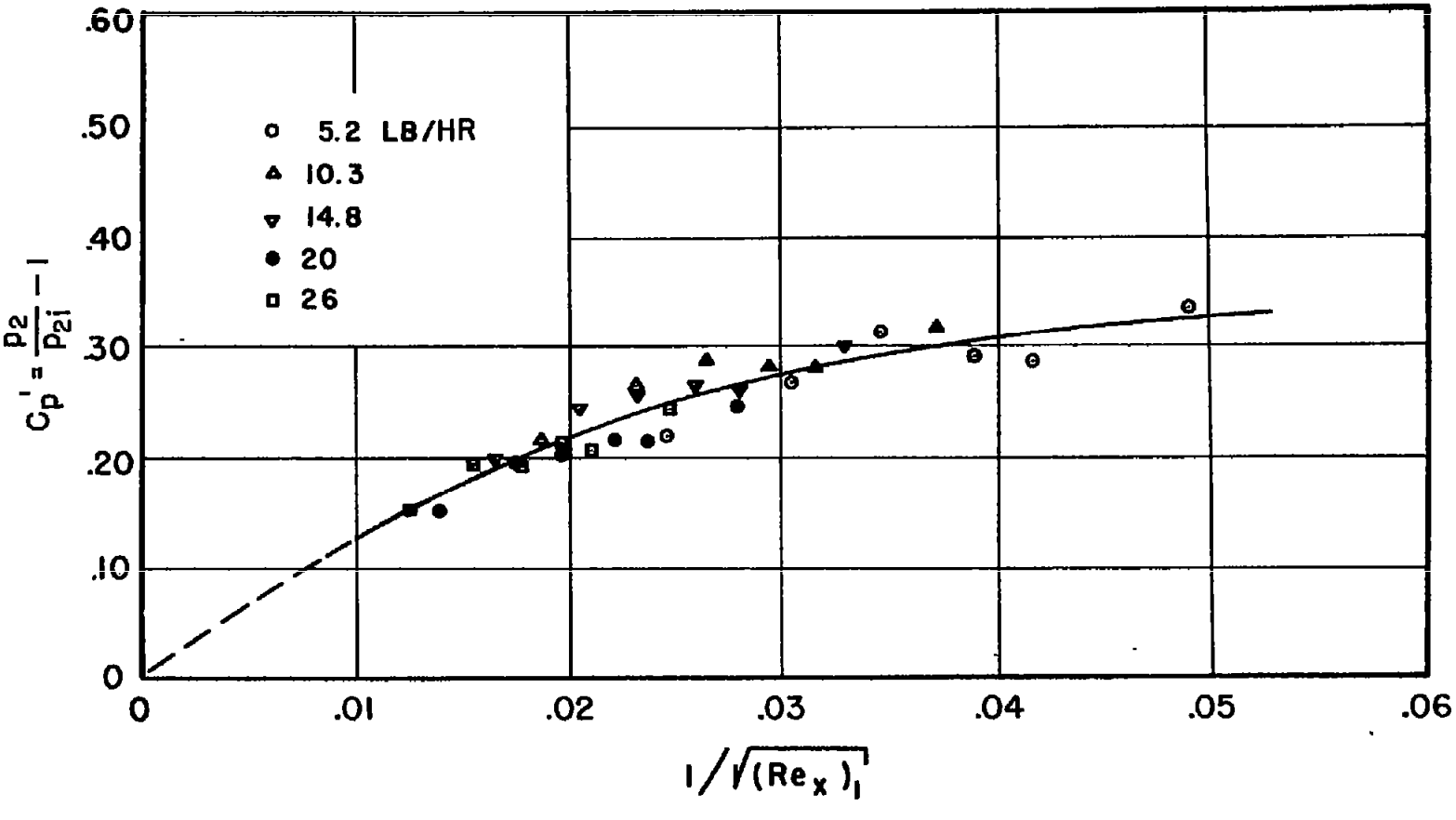

Figure 7.- Pressure coefficients for geometrically similar cones (type B models). Nozzle 8; $3.69 < M_1 < 4.13$.

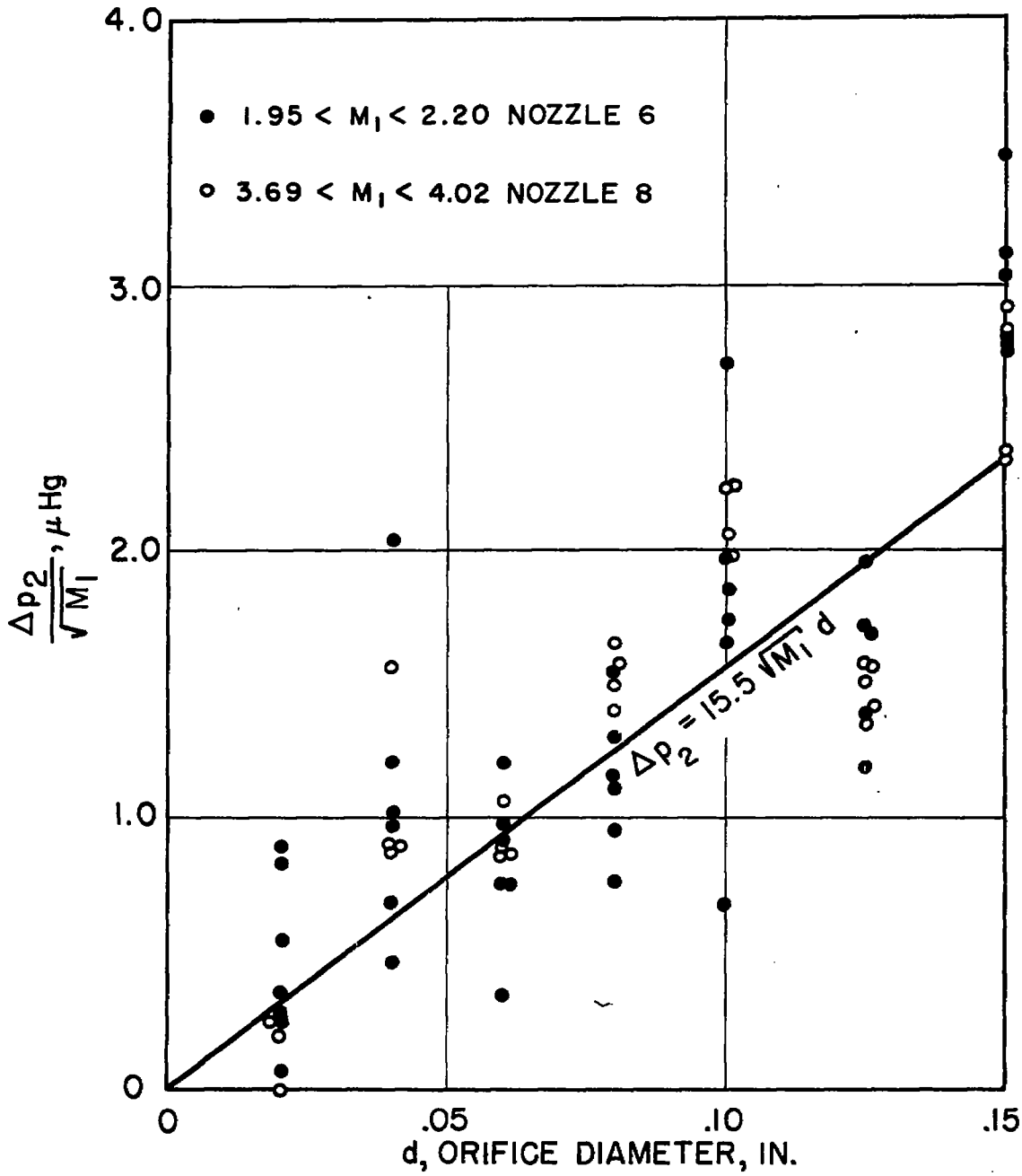

Figure 8.- Orifice size effect. Type C models.

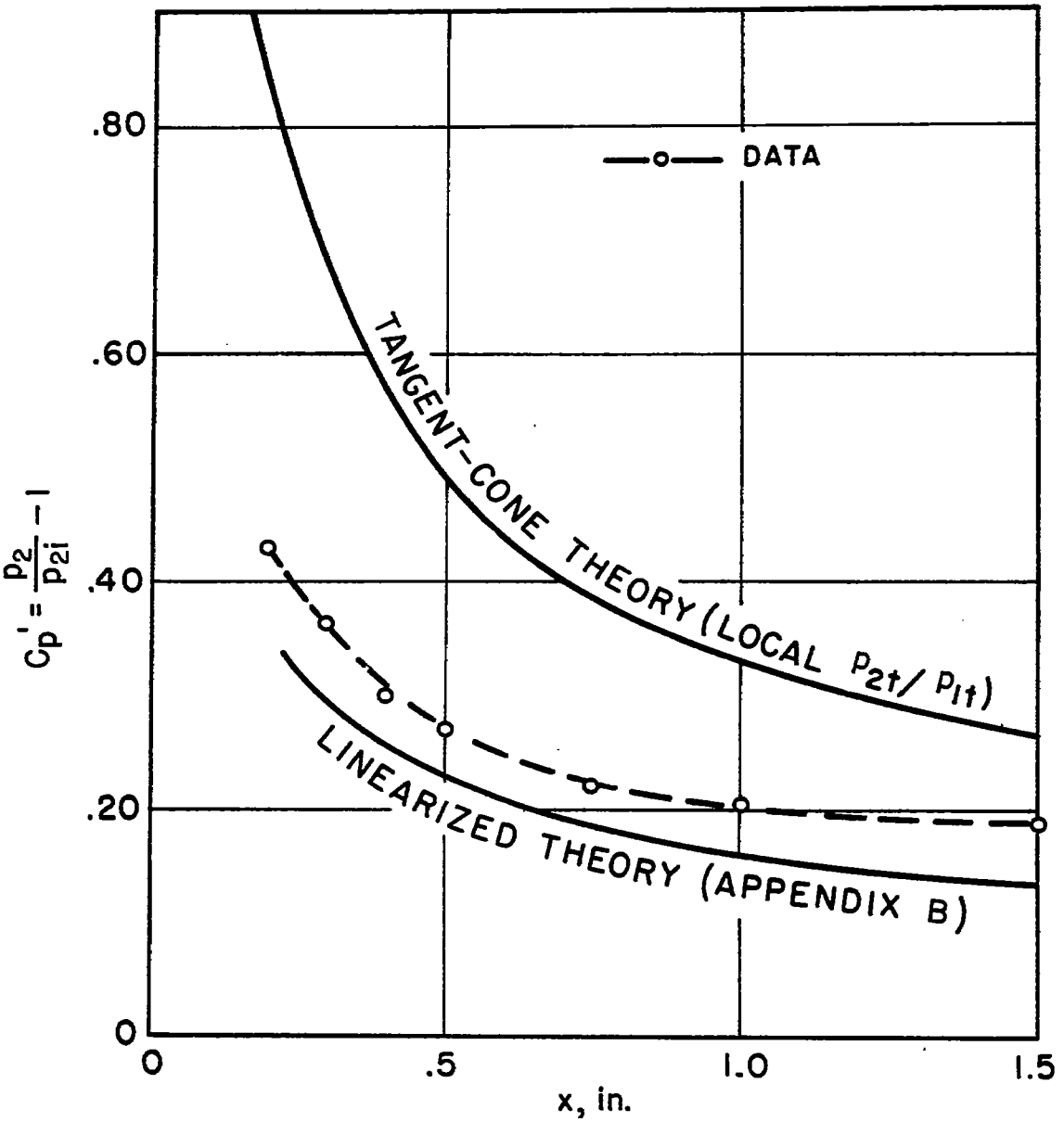

Figure 9.- Comparison between tangent-cone and linearized theories. Nozzle 8; $M_1 = 3.70$; $Re_1/inch = 929$.

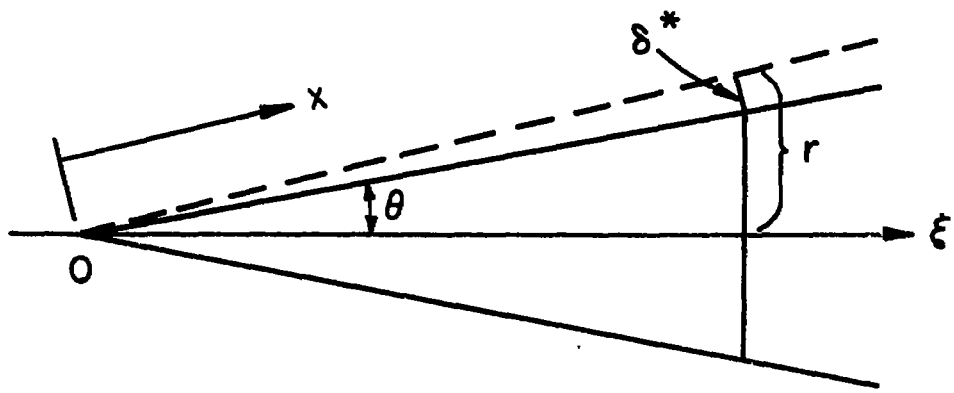

Figure 10.- Cone geometry.

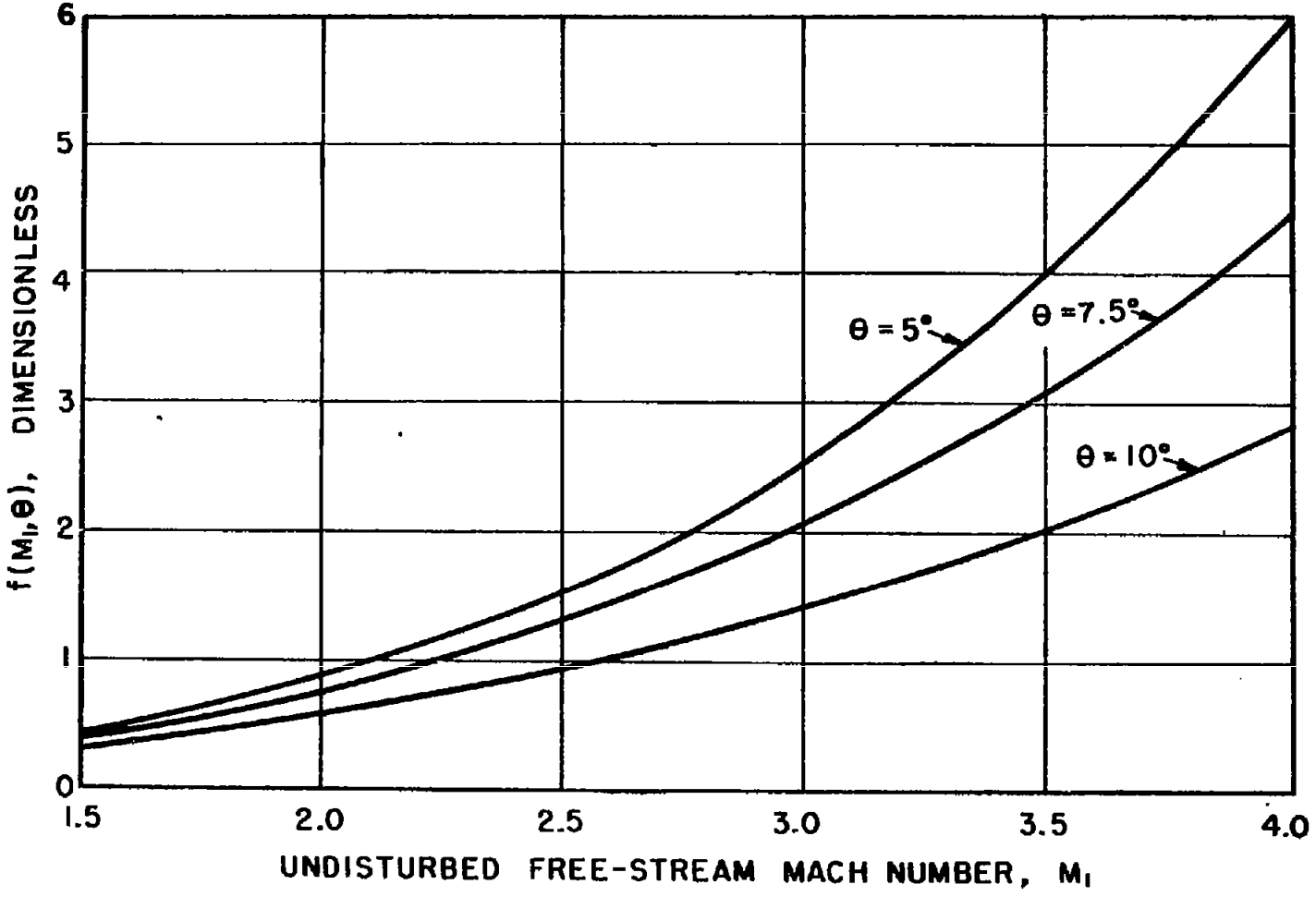

Figure 11.- Effect of boundary layer on cone surface pressure in supersonic flow. Linearized theory; $C_p' = p_2/p_{2i} - 1 = \frac{f(M_1,\theta)}{\sqrt{(Re_x)_2}}$.